Band gap tuning of layered III-Te materials

Jimena Anahí Olmos-Asar, Cedric Rocha Leão, and Adalberto Fazzio

Citation: Journal of Applied Physics **124**, 045104 (2018); doi: 10.1063/1.5021259
View online: https://doi.org/10.1063/1.5021259
View Table of Contents: http://aip.scitation.org/toc/jap/124/4
Published by the American Institute of Physics

Band gap tuning of layered III-Te materials

Jimena Anahí Olmos-Asar,[1,2,a)] Cedric Rocha Leão,[1] and Adalberto Fazzio[3]
[1]*Universidade Federal do ABC, Santo André, São Paulo, Brazil*
[2]*INFIQC, CONICET, Departamento de Química Teórica y Computacional, Facultad de Ciencias Químicas, Universidad Nacional de Córdoba, X5000HUA Córdoba, Argentina*
[3]*Brazilian Nanotechnology National Laboratory (LNNano), CNPEM, 13083-970 Campinas, Brazil*

(Received 2 January 2018; accepted 27 June 2018; published online 24 July 2018)

Gallium telluride is a layered material with high photoresponse and is very promising for applications in optoelectronic devices such as photovoltaic cells or radiation detectors. We analyze how the properties of thin films of this material scale with its thickness and also study two other proposed materials with the same crystalline structure whose room-temperature stability we verify. We show that electronic band gaps up to 2.16 eV can be obtained by stacking up and/or applying perpendicular electric field to these III-Te monolayers. This form of band gap engineering may be promising for several technological applications. *Published by AIP Publishing*. https://doi.org/10.1063/1.5021259

I. INTRODUCTION

The development of the electronic industry heavily relies on techniques to engineer semiconductors and tune their properties for specific applications. An important example that has already encountered commercial application is the strained semiconductor technology, in which thin films of silicon are grown over a substrate—usually SiGe. The strain produced on silicon due to lattice mismatch results mostly in an increase in the mobility of electrons and holes in the material, improving its performance in MOSFETs.[1–4] Another example is band gap tuning on perovskites to improve their performance in solar cells.[5–8]

In recent years, an even more ambitious strategy has been sought: designing and synthesizing materials not known to exist in nature. The unquestionable success of the simulation of properties of matter by means of quantum mechanical calculations has been promoting a shift in its original aim from descriptive to becoming a predictive tool (see, for example, Ref. 9 and references therein). Allying the vast databases of material properties with complex computer algorithms to browse through and group different elements, several initiatives across the world intend to design new materials first in the computer and then synthesize them in the laboratories. After a new material is drafted from a combination of different elements in a given crystalline structure and is predicted to present optimal properties for a certain application (photovoltaics, ion batteries, memristors, etc.), further computer simulations are needed to verify whether the proposed structure is stable. Only then, intensive experimental efforts will be made to try to actually grow the new structure. This innovative approach in materials science, although still incipient, is expected to play a major role in the near future.

In this work, we combine both strategies—materials design and engineering—to propose 2D structures for efficient optoelectronic applications. Inspired by a known layered semiconductor with promising optoelectronic characteristics—gallium telluride—we investigate how the properties of III-Te thin films can be tuned. In particular, we study how the electronic features are modified by the variations in the amount of layers in the films, as well as by the application of an external electric field.

GaTe layers can be exfoliated from bulk with the scotch-tape method,[10] intensively applied in graphene obtention.[11,12] They can also be synthesized through chemical vapor deposition (CVD) on mica substrates.[13] As one of the most representative members of the planar low-symmetry 2D materials,[14] this semiconductor has won much attention in the recent years.[10,15,16] With a moderate direct band gap of $\sim$1.7 eV, responsible for its high absorption coefficient and efficient electron-hole pair generation under photoexcitation, GaTe has demonstrated to have high photoresponsivity and small response times in photodetectors. Among its several possible applications solar cells, radiation detectors and thermoelectric devices[14,17–22] are particularly promising. For the specific case of radiation detection, the high average atomic number of GaTe and its densely packed crystal structure confer it high stopping power for very energetic photons; that is, its dense electrosphere combined with the compact atomic structure maximizes the probability of high energy photons being captured by the material.

We also study these processes in two other materials not yet synthesized but whose viability we discuss: monolayer and few layer InTe and TlTe, both with the same atomic arrangement as GaTe. Because of the much higher average atomic number, these materials could perform even better than GaTe in terms of photon absorption, especially high energy ones. Like GaTe, however, they would retain the possibility of having their electronic behavior adjusted by changing the stacking of the layers and by the application of perpendicular electrical fields.

II. METHODS AND COMPUTATIONAL DETAILS

A. Electronic structure calculations

Calculations were made within the density functional theory (DFT) approach[23] using the Vienna *Ab-initio* Simulation Package,[24,25] with the Projector-Augmented Wave method[26]

[a)]jimenaolmos@gmail.com

to represent the interaction between valence electrons and ions and with an energy cutoff of 425 eV for the selection of the plane waves. Exchange and correlation are described through the generalized gradient approximation in the Perdew-Burke-Ernzerhof (PBE)[27] implementation. The first Brillouin zone was sampled with a $10 \times 2 \times 1$ grid centered at the Γ point. Enough vacuum was added in the perpendicular direction to avoid spurious interaction between periodic images, and in relaxations, all the atoms were allowed to move until the individual forces were smaller than 0.01 eV $Å^{-1}$. van der Waals interactions were introduced by the DF-vdW method proposed by Dion *et al.*,[28] in the optB86b-vdW version.[29] As PBE is known to underestimate the electronic band gap of several semiconductors, we used HSE06 hybrid functional[30] to correct the values for the monolayers.

B. Molecular dynamics

DFT molecular dynamics simulations were performed with the CP2K open source software.[31] The pseudopotentials of Goedecker, Teter, and Hutter[32–34] with 13 electrons for Ga, In, and Tl and 6 electrons for Te were used. All calculations were made on 7×1 supercells at the Γ point, with cutoffs of 5442/680 eV for the finest grid/relative grid for Gaussian mapping and using DZVP basis functions.[35] All the simulations were done in the canonical ensemble with velocity rescaling for temperature control. The molecular dynamics consisted of 10 ps of thermalization, and a production run of 20 ps afterwards, with a reduction in the velocity rescaling by a factor of 10. Short NPT simulations were performed as well to validate the results.

III. RESULTS AND DISCUSSION

Gallium telluride monolayer has been obtained and characterized experimentally.[10,13] Parameter free computer simulations confirm that this structure is thermodynamically stable, as well as InTe and TlTe monolayers with the same atomic arrangement as GaTe, which have not been experimentally achieved yet.[36] The formation energies of these systems can be estimated as

$$E_f = \frac{E_{III-Te} - 12E_{III_{bulk}} - 12E_{Te_{bulk}}}{24}. \quad (1)$$

In this equation, E_{III-Te} is the total energy of the system, $E_{III_{bulk}}$ and $E_{Te_{bulk}}$ are the energies of single atoms in the most stable bulk phase. We show the results for the three monolayers in Table I. The dynamic stability of these systems can also be estimated through analysis of phonon modes. We have not found negative phonon frequencies in the simulated spectra of neither one of these three monolayers. With these data, we conclude that all of them are viable structures.

TABLE I. III-Te monolayers properties. Data show formation energy per atom [from Eq. (1)] and electronic band gap: without and with SOC using PBE functional, and without SOC using HSE06 hybrid functionals.

Material	E_f (eV/at)	E_g – PBE (eV)	E_g w SOC – PBE (eV)	E_g – HSE06 (eV)
GaTe	−0.371	1.46	1.38	2.16
InTe	−0.340	1.39	1.27	1.99
TlTe	−0.061	0.68	0.53	1.06

On the other hand, it is possible to define the formation energy of a 2D material relative to the bulk ground-state phase as

$$\Delta E_f = \frac{E_{2D}}{N_{2D}} - \frac{E_{3D}}{N_{2D}}, \quad (2)$$

where E_{2D} and E_{3D} are the total energies of the 2D and 3D structures, respectively, and N_{2D} and N_{3D} are the numbers of atoms in the 2D and 3D unit cells.[37] In the case of GaTe, the reference 3D structure is the most stable monoclinic layered bulk. We obtain a value of 61 meV/atom. By definition, a positive energy means that the 2D structure is less stable than the 3D one, and the smaller this energy, the more probable it can be formed. The obtained value is in the order of previous results for different 2D systems.[38] For the cases of InTe and TlTe, we obtain ΔE_f equal to -30 meV/at and 187 meV/at, respectively. The reason why the 2D structure of InTe is more stable than the 3D structure is that the bulk with this stoichiometry is unstable (it decomposes to In_4Te_3 and In_7Te_{10}). 2D TlTe has the largest formation energy with respect to the 3D bulk and is less likely to be formed.

One question that arises is whether these materials in the proposed structures are stable at room temperature, especially TlTe, which has a quite small (still negative) formation energy, as indicated in Table I. This is an important point for real technological applications. For this reason, we have studied the thermal stability of the monolayers; that is, we observe their structural parameters when increasing the temperature, at constant volume. We performed molecular dynamics simulations at two different temperatures: 300 and 500 K. The radial distribution function g(r) (for III-Te, III-III, and Te-Te pairs), at both scenarios, is shown in Fig. 1. g(r) at 0 K is also shown as a reference. For GaTe and InTe, there are not significant changes between the two thermal conditions, meaning that they should remain stable at typical operational setups. However, for TlTe a liquid phase is observed already at 500 K, and this fact could represent a difficulty for some above-room-temperature technological applications.

Even though bidimensional systems could release the strain in the other direction, one should also perform NPT simulations in order to check that the main conclusions are valid. In the supplementary material, we present data which confirm that the NVT results are correct.

In order to aid experimentalists trying to synthesize these monolayers, in Fig. 2 we simulate the power spectra of these three 2D materials at 300 K. As expected due to the differences in masses, GaTe shows vibrational modes at higher frequencies, while TlTe should not present any absorption above 150 cm^{-1}. As previously mentioned, no negative frequencies are expected for any of the monolayers.

Given that GaTe, InTe, and TlTe are shown to be stable and solid at room temperature, we investigated their electronic properties. We found that the band gap is direct for the three systems, diminishing as the atomic number of the

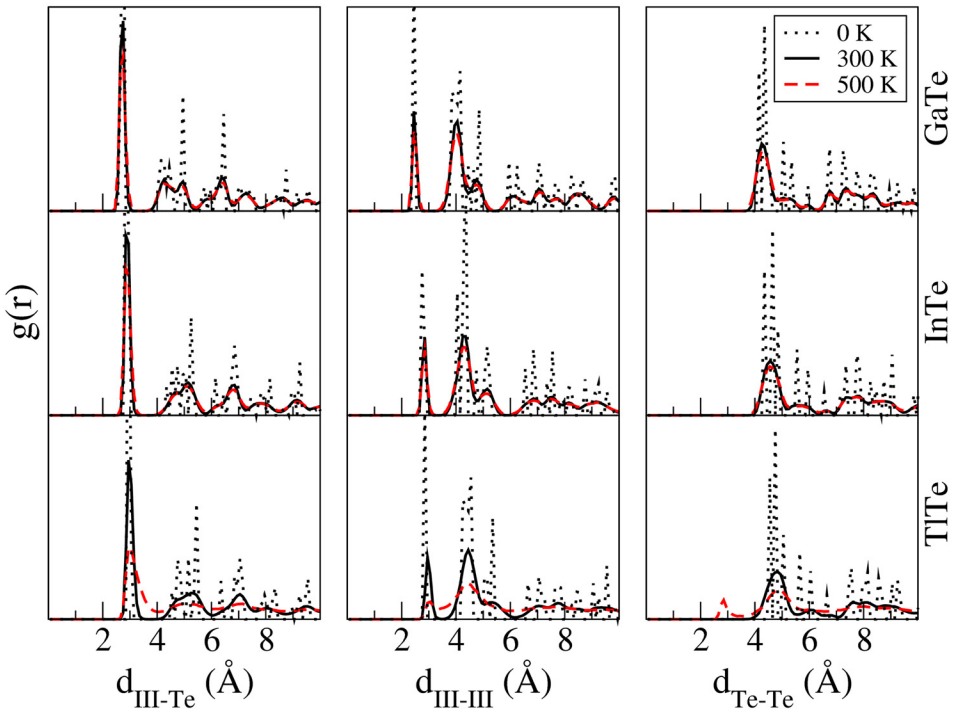

FIG. 1. Radial distribution function (g(r)) for III-Te monolayers at 300 (continuous black) and 500 (dashed red) K. The 0 K condition (dotted black) is shown as a reference.

cation increases, as indicated in Table I. In Fig. 3, we show the atomic structure, first Brillouin zone, band structures, band alignment with respect to vacuum, and the imaginary part of the dielectric constant for the three materials. The inclusion of spin orbit coupling (SOC) in the calculations practically does not modify the results. As can be deduced from the dielectric constants, the optical absorption of the monolayers covers a wide range of radiation (between 1 to 5 eV, approximately).

One may ask about whether any of these monolayers fit in type II topological insulators (TIs). Type II TIs are not limited to the honeycomb lattice, which is clearly not the case for the III-Te monolayers we are investigating here. For type II TIs, the mechanism is band inversion and parities exchange at time-reversal symmetry points.[39] To reveal the topological class of these insulators, we calculated the z2 invariant by performing full-relativistic calculations and using the Z2Pack,[40] which follows the method proposed by Soluyanov and Vanderbilt.[41] We found that the materials are trivial insulators with $z2 = 0$.

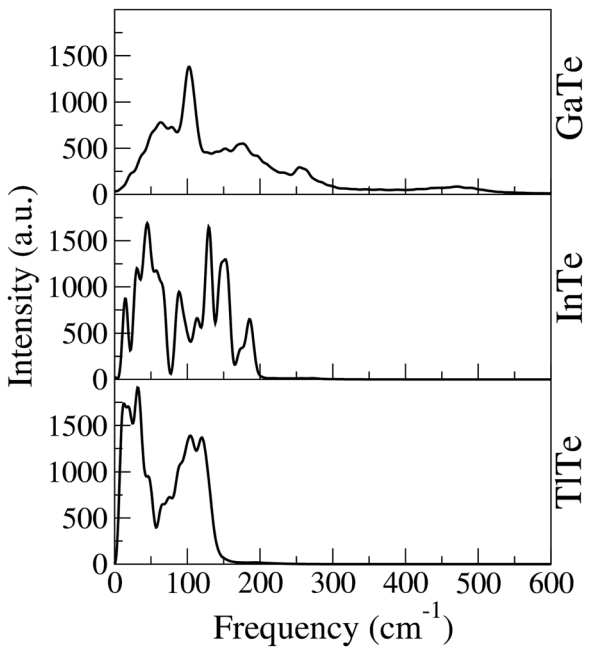

FIG. 2. Power spectra for III-Te monolayers at 300 K.

Monolayers are the smallest building blocks for heterostructures formation, and that is why studying their properties is of great importance. However, in some technological applications III-Te multilayers are more likely to be present in the device instead of monolayers. This could happen due to experimental limitations, for example, or as a strategy to maximize the radiation absorption. In any case, it is interesting to study how the properties of the materials change as they get thicker. With this purpose, we have simulated III-Te films with 2 to 5 layers. For all the systems, the energy band gap decreases as the size of the film increases, as expected. In the cases of GaTe and InTe, the direct character of the band gap is conserved up to 5 layers, while for TlTe, the gap becomes indirect already for the bilayer. This may result in the loss of efficiency for light absorption near the band gap for this material. The values of the band gaps are listed in Table II.

As the system grows the absorption is expected to increase, improving the efficiency of the device. In Fig. 4, the imaginary part of the dielectric constant in the xx direction is shown for the three materials. In general, the absorption increases with the film's thickness, while the wavelength of the maximum remains almost constant. It is interesting to note that in the case of TlTe, there are two maxima for optical absorption: one around 2.5 eV, in the visible part of the spectrum, and the other around 5 eV. This is due to the existence of an intrinsic unoccupied intermediate

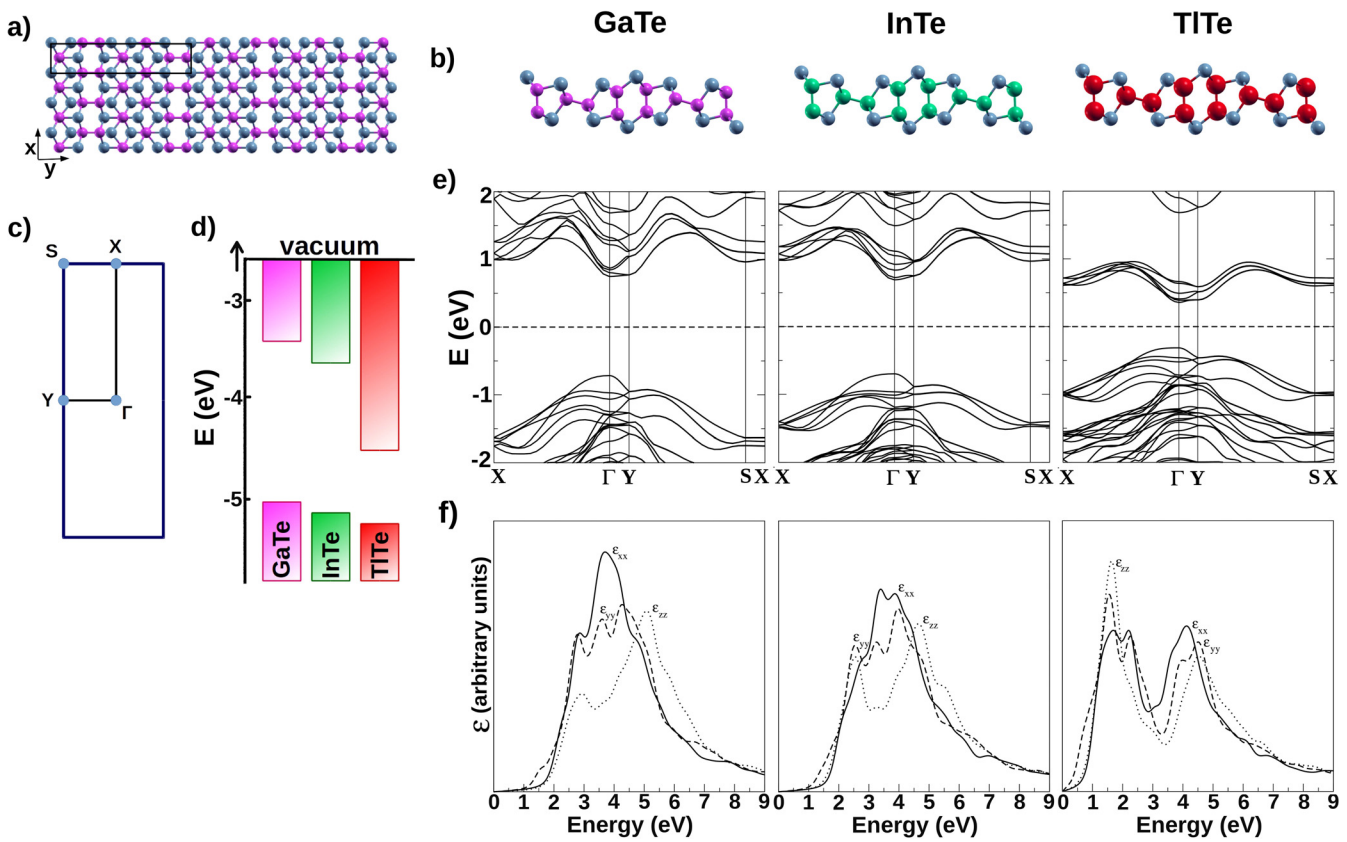

FIG. 3. III-Te monolayers properties (a) top view of GaTe; in black, a unit cell is delimited; (b) side view of all III-Te monolayers; pink: Ga atoms; green: In; red: Tl; blue: Te (c) first Brillouin zone (d) band alignment with respect to vacuum (within the PBE approximation); (e) electronic band structures; (f) imaginary part of the dielectric constants as a function of energy.

band separating the valence band (VB) maximum from another unoccupied band at higher energies. The existence of two band gaps could improve radiation absorption when the material is applied in technological devices, such as solar cells. This is due to an increase in the range of the spectrum that they can absorb; photons with insufficient energy to pump electrons from the valence band to the conduction band can use this intermediate band to generate an electron–hole pair.[42,43]

The interlayer energy per atom for a system containing n layers can be calculated as

$$E_{int} = \frac{E_{III-Te_n} - nE_{III-Te}}{N}, \tag{3}$$

where E_{III-Te_n} is the energy of the III-Te multilayer, E_{III-Te} is the energy of the monolayer, and N is the number of atoms in the system. This interlayer energy increases as the systems grow, and the interaction is the strongest for TlTe (see Table II). This could be explained by the atomic charges on each material. For the case of TlTe, the tellurium ions have a charge of ~ -0.2 e, while Te ions on GaTe and InTe have a charge of ~ -0.4 e. Since in all cases Te atoms are on the outer side of the layer, the smaller charge observed on TlTe relative to these two latter structures indicates less interlayer repulsion. In fact, the interlayer distance for TlTe is shorter than for GaTe and InTe. Our results, then, suggest that the exfoliation energy in these systems is on the order of tens of meV, meaning that the obtention of single or few monolayers is feasible with relative ease experimentally (Table II).

TABLE II. Structural and electronic properties of III-Te multilayers. Values show the interlayer energy per atom and the energy band gaps.

	GaTe		InTe		TlTe	
n	E_{int} (eV/at)	E_g (eV)	E_{int} (eV/at)	E_g (eV)	E_{int} (eV/at)	E_g (eV)
2	−0.037	1.25	−0.041	1.13	−0.051	0.35
3	−0.049	1.12	−0.055	1.02	−0.069	0.17
4	−0.056	1.07	−0.063	0.96	−0.078	0.05
5	−0.059	1.04	−0.067	0.92	−0.084	0.03

As mentioned before, E_g decreases as the number of layers increases. We can predict how the band gap of a system with n layers scales using the following equation:

$$E_g = E_0 + \frac{a}{n^b}, \tag{4}$$

where a and b are constants. The monolayer does not fit in this trend, probably due to the lack of interlayer coupling.[44] We thus expect it to be followed by III-Te systems from 2 to n layers. As the thickness of the film goes to infinity, E_g in Eq. (4) tends to E_0. Therefore, E_0 in the case of GaTe coincides with the material's bulk ($n \to \infty$) band gap. For layered InTe and TlTe thin films, E_0 is simply the asymptotic limit of the curves with no physical meaning, since the corresponding bulk phases do not exist in principle. In Fig. 5(a), we show the energy band

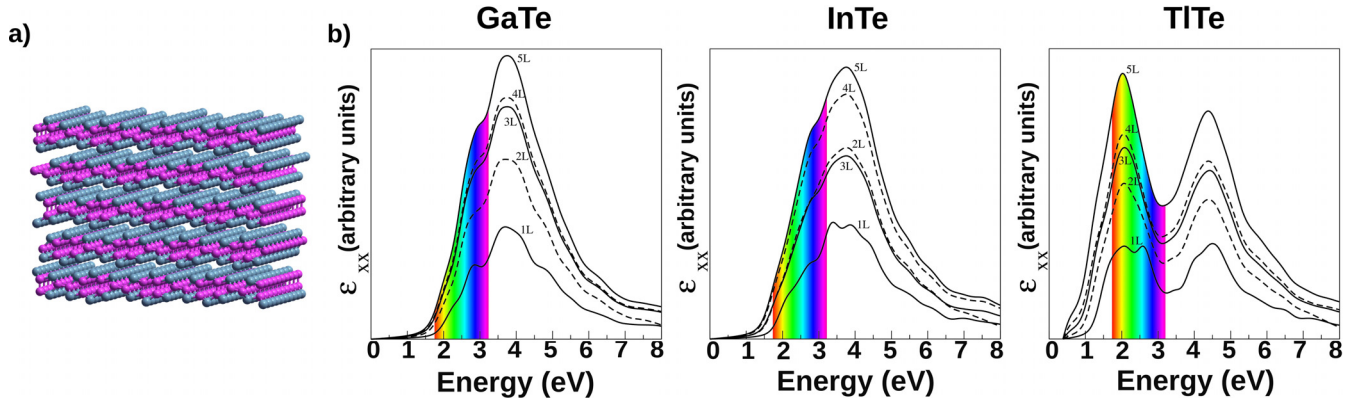

FIG. 4. III-Te multilayers. (a) Schematic representation of a 5L GaTe 10 × 2 supercell; color code according to Fig. 3 (b) imaginary part of the dielectric constant in the xx direction for 1 to 5 layers. The visible part of the spectrum is depicted.

gaps for III-Te systems with 2 to 5 layers, as well as the fitting made according to Eq. (4). See Table III for fitted constants.

Finally, in addition to the stacking layers of material, another way to tune the electronic band gap of a semiconductor is through the application of an external electric field. This method is more effective in thin films. The possibility to tune the band gap of materials via the application of a transverse electric field could be interesting in several implementations of devices composed by different materials. For example, a single LED color could be changed by the application of the electric field. Another example would be in radiation detectors. One important factor for noise that impairs the accurate measurement, and thus the identification of the source of radiation, is called Fano noise.[45] This is related to the low statistics of absorbed photons, an effect that increases as the band gap increases relative to the energy of the incoming radiation. On the other hand, small band gaps introduce other sources of loss, such as dark or leakage current. Thus, modulating the band gap of the material in a radiation detection device by the application of an electric field could enable it to be used in medical applications, detecting X-rays, in astronomical applications and even in national defense, detecting materials producing gamma radiation.

We have simulated a single monolayer of each material during the application of a perpendicular electric field of increasing intensity. As can be observed in Fig. 5(b), for InTe and TlTe, when increasing the field the band gap decreases slowly at first but starts to decay faster for larger electric fields. In the case of GaTe, the band gap reduction is faster, and the system becomes metallic already at 0.8 eV/Å. To try to understand these different behaviors, we have analyzed the changes produced by the applied electric field from two different approaches: (i) analyzing the electronic levels and (ii) studying the spatial charge distribution before and after electric field application.

(i) First we note that in the cases of InTe and TlTe, there exists a pseudo-gap in the conduction band (CB). This gap is more clear in the case of TlTe (indeed, we say that it has an intermediate band), but it still can be spotted in InTe, although less separated from the upper levels. Also, the character of the levels at the band edges are different: For GaTe and InTe, the top of the valence band (VB) is mainly p^{Te} while the bottom of the CB is mainly s^{Ga}/s^{In}, while for the case of TlTe, both the top of the VB and the bottom of the CB are mainly p^{Te} (see supplementary material). In addition, from the DOS we can clearly see how the density of levels associated with the edge states decreases when the atomic number of the cation increases. This may explain the higher response of GaTe relative to InTe and even more so to TlTe when a perpendicular electric field is applied.

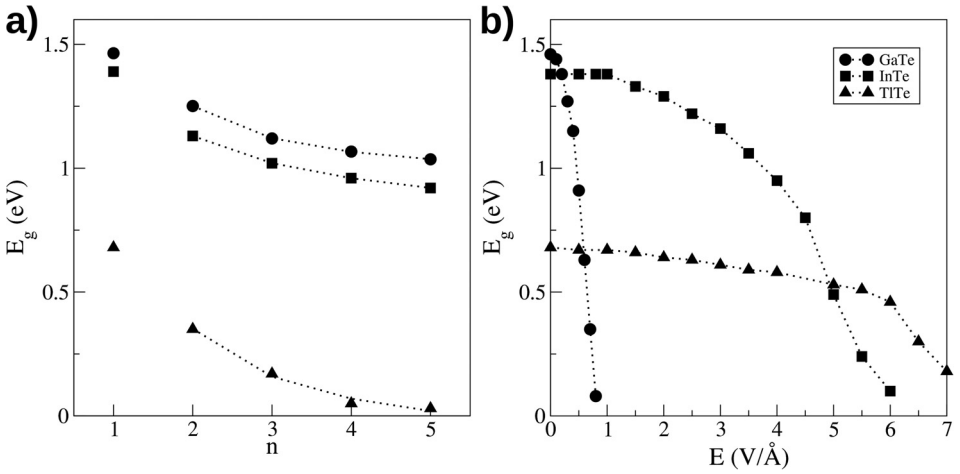

FIG. 5. Energy band gaps. (a) E_g as a function of the number of layers; the dotted lines are the fittings made according to Eq. (4); (b) E_g for a monolayer under the effect of different perpendicular electric fields.

TABLE III. E_0 (known for GaTe and fitted from the data for InTe and TlTe) and a and b fitted constants, according to Eq. (4).

Material	E_0 (eV)	a (eV)	b
GaTe	0.96 (calculated)	0.80	1.46
InTe	0.69	0.72	0.71
TlTe	−0.13	1.16	1.25

(ii) The second analysis is based on the spatial distribution of the charge density. Taking a look at the charge density difference (please see the supplementary material) for the three monolayers before and after the field is applied, we observe two different behaviors: For InTe and TlTe, the field creates charge separation, accumulating electrons on Te at the bottom of the monolayer while decreasing the charge on the other Te atoms (Te is always in the external part of the monolayer), while for GaTe, the electric field accumulates charge on both borders of the monolayer.

The differences observed between GaTe and InTe/TlTe may be a combination of the energetic localization of the levels both, at the valence and conduction band, and the spatial arrangement of charges when the field is applied.

If we extrapolate the band gap versus electric field curves, we can predict a breakdown voltage for each monolayer: ∼0.8 for GaTe, ∼6.5 for InTe, and more than 7.0 for TlTe. Application of electric fields has been found to induce topological phases in 2D materials.[46] In the case of GaTe, we observe a band inversion on the last occupied levels, yet the parity is conserved, so no topological phase is achieved for these systems.

As can be extracted from Fig. 5, the band gaps of III-Te mono- and multilayers can be tuned, ranging from metals to 1.46 eV bandgap semiconductors, depending on the chosen material, the number of layers, and the applied external electric field. This could be a promising way to engineer the proper band gap for each particular purpose. It is worth mentioning that hybrid 2D materials can be created by stacking different III-Te monolayers one on top of each other, increasing the possibilities for the implementation of III-Te materials in optoelectronic devices.

IV. CONCLUSIONS

III-Te mono- and multilayers are highly photoresponsive materials and thus very promising for applications in optoelectronic devices. We have shown that InTe and TlTe monolayers with the structure GaTe, although not synthesized yet, are thermodynamically and dynamically stable and solid at room temperature. The monolayers could also be stacked forming thicker films, presenting different optical and electronic properties, tailored for specific applications and presenting a wide range of energy band gaps. We have also demonstrated that the application of a perpendicular electric fields in these materials allow the obtention of band gaps that span an interval between 0.00 and 1.46 eV, covering a wide range of the radiation spectrum. These findings open the possibility to integrate these materials in several forms and combinations in technological devices, such as solar cells and radiation detectors.

SUPPLEMENTARY MATERIAL

See supplementary material for electronic band structures, charge density differences, and DOS for the cases with an external electric field. In addition, selected snapshots and cell parameters extracted from the NPT molecular dynamics simulations.

ACKNOWLEDGMENTS

This work was financed by Fundaçãde Amparo á Pesquisa do estado de São Paulo (FAPESP), Conselho Nacional de Desenvolvimento Científico e Tecnológico (CNPq), and Coordenação de Aperfeiçoamento de Pessoal de Nível Superior (CAPES). J.A.O.-A. thanks FAPESP for a fellowship (process n. 2016/12021-0) and CONICET.

[1]E. Parton and P. Verheyen, "Strained silicon—The key to sub-45 nm cmos," III-Vs Rev. **19**, 28–31 (2006).
[2]S. E. Thompson, M. Armstrong, C. Auth, S. Cea, R. Chau, G. Glass, T. Hoffman, J. Klaus, Z. Ma, B. Mcintyre, A. Murthy, B. Obradovic, L. Shifren, S. Sivakumar, S. Tyagi, T. Ghani, K. Mistry, M. Bohr, and Y. El-Mansy, "A logic nanotechnology featuring strained-silicon," IEEE Electron Device Lett. **25**, 191–193 (2004).
[3]T. Ghani, M. Armstrong, C. Auth, M. Bost, P. Charvat, G. Glass, T. Hoffmann, K. Johnson, C. Kenyon, J. Klaus, B. McIntyre, K. Mistry, A. Murthy, J. Sandford, M. Silberstein, S. Sivakumar, P. Smith, K. Zawadzki, S. Thompson, and M. Bohr, "A 90 nm high volume manufacturing logic technology featuring novel 45 nm gate length strained silicon cmos transistors," in *Proceedings of the IEEE International Electron Devices Meeting* (2003), pp. 11.6.1–11.6.3.
[4]K. Mistry, C. Allen, C. Auth, B. Beattie, D. Bergstrom, M. Bost, M. Brazier, M. Buehler, A. Cappellani, R. Chau, C. H. Choi, G. Ding, K. Fischer, T. Ghani, R. Grover, W. Han, D. Hanken, M. Hattendorf, J. He, J. Hicks, R. Huessner, D. Ingerly, P. Jain, R. James, L. Jong, S. Joshi, C. Kenyon, K. Kuhn, K. Lee, H. Liu, J. Maiz, B. McIntyre, P. Moon, J. Neirynck, S. Pae, C. Parker, D. Parsons, C. Prasad, L. Pipes, M. Prince, P. Ranade, T. Reynolds, J. Sandford, L. Shifren, J. Sebastian, J. Seiple, D. Simon, S. Sivakumar, P. Smith, C. Thomas, T. Troeger, P. Vandervoorn, S. Williams, and K. Zawadzki, "A 45 nm logic technology with high-k+metal gate transistors, strained silicon, 9 cu interconnect layers, 193 nm dry patterning, and 100 packaging," in *Proceedings of the IEEE International Electron Devices Meeting* (2007), pp. 247–250.
[5]R. Nechache, C. Harnagea, S. Li, L. Cardenas, W. Huang, J. Chakrabartty, and F. Rosei, "Bandgap tuning of multiferroic oxide solar cells," Nat. Photonics **9**, 61–67 (2015).
[6]M. Pandey, K. W. Jacobsen, and K. S. Thygesen, "Band gap tuning and defect tolerance of atomically thin two-dimensional organic–inorganic halide perovskites," J. Phys. Chem. Lett. **7**, 4346–4352 (2016).
[7]R. Prasanna, A. Gold-Parker, T. Leijtens, B. Conings, A. Babayigit, H.-G. Boyen, M. F. Toney, and M. D. McGehee, "Band gap tuning via lattice contraction and octahedral tilting in perovskite materials for photovoltaics," J. Am. Chem. Soc. **139**, 11117–11124 (2017).
[8]H. Hasegawa, K. Kobayashi, Y. Takahashi, J. Harada, and T. Inabe, "Effective band gap tuning by foreign metal doping in hybrid tin iodide perovskites," J. Mater. Chem. C **5**, 4048–4052 (2017).
[9]S. Curtarolo, G. L. W. Hart, M. B. Nardelli, N. Mingo, S. Sanvito, and O. Levy, "The high-throughput highway to computational materials design," Nat. Mater. **12**, 191 (2013).
[10]F. Liu, H. Shimotani, H. Shang, T. Kanagasekaran, V. Zólyomi, N. Drummond, V. I. Fal'ko, and K. Tanigaki, "High-sensitivity photodetectors based on multilayer gate flakes," ACS Nano **8**, 752–760 (2014).
[11]K. S. Novoselov, A. K. Geim, S. V. Morozov, D. Jiang, Y. Zhang, S. V. Dubonos, I. V. Grigorieva, and A. A. Firsov, "Electric field effect in atomically thin carbon films," Science **306**, 666–669 (2004).

[12]K. S. Novoselov, D. Jiang, F. Schedin, T. J. Booth, V. V. Khotkevich, S. V. Morozov, and A. K. Geim, "Two-dimensional atomic crystals," Proc. Natl. Acad. Sci. U.S.A. **102**, 10451–10453 (2005).
[13]Z. Wang, M. Safdar, M. Mirza, K. Xu, Q. Wang, Y. Huang, F. Wang, X. Zhan, and J. He, "High-performance flexible photodetectors based on gate nanosheets," Nanoscale **7**, 7252–7258 (2015).
[14]S. Huang, Y. Tatsumi, X. Ling, H. Guo, Z. Wang, G. Watson, A. A. Puretzky, D. B. Geohegan, J. Kong, J. Li, T. Yang, R. Saito, and M. S. Dresselhaus, "In-plane optical anisotropy of layered gallium telluride," ACS Nano **10**, 8964–8972 (2016).
[15]J. J. Fonseca, S. Tongay, M. Topsakal, A. R. Chew, A. J. Lin, C. Ko, A. V. Luce, A. Salleo, J. Wu, and O. D. Dubon, "Bandgap restructuring of the layered semiconductor gallium telluride in air," Adv. Mater. **28**, 6465–6470 (2016).
[16]U. S. Shenoy, U. Gupta, D. S. Narang, D. J. Late, U. V. Waghmare, and C. Rao, "Electronic structure and properties of layered gallium telluride," Chem. Phys. Lett. **651**, 148–154 (2016).
[17]J. Susoma, L. Karvonen, A. Säynätjoki, S. Mehravar, R. A. Norwood, N. Peyghambarian, K. Kieu, H. Lipsanen, and J. Riikonen, "Second and third harmonic generation in few-layer gallium telluride characterized by multi-photon microscopy," Appl. Phys. Lett. **108**, 073103 (2016).
[18]S. Pal and D. Bose, "Growth, characterisation and electrical anisotropy in layered chalcogenides GaTe and InTe," Solid State Commun. **97**, 725–729 (1996).
[19]D. N. Bose and S. Pal, "Photoconductivity, low-temperature conductivity, and magnetoresistance studies on the layered semiconductor gate," Phys. Rev. B **63**, 235321 (2001).
[20]Y. Cui, D. D. Caudel, P. Bhattacharya, A. Burger, K. C. Mandal, D. Johnstone, and S. A. Payne, "Deep levels in gate and gate: In crystals investigated by deep-level transient spectroscopy and photoluminescence," J. Appl. Phys. **105**, 053709 (2009).
[21]A. J. Nelson, A. M. Conway, B. W. Sturm, E. M. Behymer, C. E. Reinhardt, R. J. Nikolic, S. A. Payne, G. Pabst, and K. C. Mandal, "X-ray photoemission analysis of chemically treated gate semiconductor surfaces for radiation detector applications," J. Appl. Phys. **106**, 023717 (2009).
[22]C. Rocha Leão and V. Lordi, "Ab initio," Phys. Rev. B **84**, 165206 (2011).
[23]P. Hohenberg and W. Kohn, "Inhomogeneous electron gas," Phys. Rev. **136**, B864–B871 (1964).
[24]G. Kresse and J. Hafner, "Ab initio molecular dynamics for liquid metals," Phys. Rev. B **47**, 558–561 (1993).
[25]G. Kresse and J. Furthmüller, "Efficient iterative schemes for ab initio total-energy calculations using a plane-wave basis set," Phys. Rev. B **54**, 11169–11186 (1996).
[26]P. E. Blöchl, "Projector augmented-wave method," Phys. Rev. B **50**, 17953–17979 (1994).
[27]J. P. Perdew, K. Burke, and M. Ernzerhof, "Generalized gradient approximation made simple," Phys. Rev. Lett. **77**, 3865–3868 (1996).
[28]M. Dion, H. Rydberg, E. Schröder, D. C. Langreth, and B. I. Lundqvist, "Van der waals density functional for general geometries," Phys. Rev. Lett. **92**, 246401 (2004).
[29]J. Klimeš, D. R. Bowler, and A. Michaelides, "Chemical accuracy for the van der waals density functional," J. Phys.: Condens. Matter **22**, 022201 (2010).
[30]J. Paier, M. Marsman, K. Hummer, G. Kresse, I. C. Gerber, and J. G. Ángyán, "Screened hybrid density functionals applied to solids," J. Chem. Phys. **124**, 154709 (2006).
[31]J. Hutter, M. Iannuzzi, F. Schiffmann, and J. VandeVondele, "cp2k: Atomistic simulations of condensed matter systems," Wiley Interdiscip. Rev.: Comput. Mol. Sci. **4**, 15–25 (2014).
[32]S. Goedecker, M. Teter, and J. Hutter, "Separable dual-space Gaussian pseudopotentials," Phys. Rev. B **54**, 1703–1710 (1996).
[33]C. Hartwigsen, S. Goedecker, and J. Hutter, "Relativistic separable dual-space Gaussian pseudopotentials from H to Rn," Phys. Rev. B **58**, 3641–3662 (1998).
[34]M. Krack, "Pseudopotentials for Hto Kr optimized for gradient-corrected exchange-correlation functionals," Theor. Chem. Acc. **114**, 145–152 (2005).
[35]J. VandeVondele and J. Hutter, "Gaussian basis sets for accurate calculations on molecular systems in gas and condensed phases," J. Chem. Phys. **127**, 114105 (2007).
[36]J. A. Olmos-Asar, C. R. Leao, and A. Fazzio, "Novel iii-te-graphene van der waals heterojunctions for optoelectronic devices," RSC Adv. **7**, 32383–32390 (2017).
[37]H. L. Zhuang and R. G. Hennig, "Electronic structures of single-layer boron pnictides," Appl. Phys. Lett. **101**, 153109 (2012).
[38]B. C. Revard, W. W. Tipton, A. Yesypenko, and R. G. Hennig, "Grand-canonical evolutionary algorithm for the prediction of two-dimensional materials," Phys. Rev. B **93**, 054117 (2016).
[39]L. Kou, Y. Ma, Z. Sun, T. Heine, and C. Chen, "Two-dimensional topological insulators: Progress and prospects," J. Phys. Chem. Lett. **8**, 1905–1919 (2017).
[40]D. Gresch, G. Autès, O. V. Yazyev, M. Troyer, D. Vanderbilt, B. A. Bernevig, and A. A. Soluyanov, "Z2pack: Numerical implementation of hybrid Wannier centers for identifying topological materials," Phys. Rev. B **95**, 075146 (2017).
[41]A. A. Soluyanov and D. Vanderbilt, "Computing topological invariants without inversion symmetry," Phys. Rev. B **83**, 235401 (2011).
[42]M. Y. Levy and C. Honsberg, "Absorption coefficients of intermediate-band media," J. Appl. Phys. **106**, 073103 (2009).
[43]A. K. Luque, A. Marti, and C. Stanley, "Understanding intermediate-band solar cells," Nat. Photonics **6**, 146–152 (2012).
[44]Y. Cai, G. Zhang, and Y.-W. Zhang, "Layer-dependent band alignment and work function of few-layer phosphorene," Sci. Rep. **4**, 6677 (2014).
[45]A. Owens and A. Peacock, "Compound semiconductor radiation detectors," Nucl. Instrum. Methods Phys. Res., Sect. A **531**, 18–37 (2004).
[46]Q. Liu, X. Zhang, L. B. Abdalla, A. Fazzio, and A. Zunger, "Switching a normal insulator into a topological insulator via electric field with application to phosphorene," Nano Lett. **15**, 1222–1228 (2015).